# Spin Injection and Relaxation in p -Doped ( In , Ga ) As / Ga As Quantum-Dot Spin Light-Emitting Diodes at Zero Magnetic Field

Alaa E Giba, Xue Gao, Mathieu Stoffel, Xavier Devaux, Bo Xu, Xavier Marie, Pierre Renucci, Henri Jaffrès, Jean-Marie George, Guangwei Cong, et al.

# Spin Injection and Relaxation in *p*-Doped (In, Ga)As/GaAs Quantum-Dot Spin Light-Emitting Diodes at Zero Magnetic Field

Alaa E. Giba,[1,2] Xue Gao,[1] Mathieu Stoffel,[1,†] Xavier Devaux,[1] Bo Xu,[3] Xavier Marie,[4] Pierre Renucci,[4] Henri Jaffrès,[5] Jean-Marie George,[5] Guangwei Cong,[6] Zhanguo Wang,[3] Hervé Rinnert,[1] and Yuan Lu[1,*]

[1] *Institut Jean Lamour, Université de Lorraine, CNRS UMR7198, Campus ARTEM, 2 Allée André Guinier, BP 50840, 54011 Nancy, France*

[2] *National Institute of Laser Enhanced Sciences, Cairo University, Giza 12613, Egypt*

[3] *Key Laboratory of Semiconductor Materials Science, Institute of Semiconductors, Chinese Academy of Sciences, P.O. Box 912, Beijing 100083, China*

[4] *Université de Toulouse, INSA-CNRS-UPS, LPCNO, 135 Avenue de Rangueil, F-31077 Toulouse, France*

[5] *Unité Mixte de Physique, CNRS, Thales, Université Paris-Saclay, 91767 Palaiseau, France*

[6] *Research Institute for Advanced Electronics and Photonics, National Institute of Advanced Industrial Science and Technology, Onogawa 1-16, Tsukuba, Ibaraki 305-8569, Japan*

(Received 15 June 2020; accepted 13 August 2020; published 8 September 2020)

We report on efficient spin injection in *p*-doped (In, Ga)As/GaAs quantum-dot (QD) spin light-emitting diodes (spin LEDs) under zero applied magnetic field. A high degree of electroluminescence circular polarization ($P_c$) ∼19% is measured in remanence up to 100 K. This result is obtained thanks to the combination of a perpendicularly magnetized Co-Fe-B/MgO spin injector allowing efficient spin injection and an appropriate *p*-doped (In, Ga)As/GaAs QD layer in the active region. By analyzing the bias and temperature dependence of the electroluminescence circular polarization, we evidence a two-step spin-relaxation process. The first step occurs when electrons tunnel through the MgO barrier and travel across the GaAs depletion layer. The spin relaxation is dominated by the Dyakonov-Perel mechanism related to the kinetic energy of electrons, which is characterized by a bias-dependent $P_c$. The second step occurs when electrons are captured into QDs prior to their radiative recombination with holes. The temperature dependence of $P_c$ reflects the temperature-induced modification of the QD doping, together with the variation of the ratio between the charge-carrier lifetime and the spin-relaxation time inside the QDs. The understanding of these spin-relaxation mechanisms is essential to improve the performance of spin LEDs for future spin optoelectronic applications at room temperature under zero applied magnetic field.

DOI: 10.1103/PhysRevApplied.14.034017

## I. INTRODUCTION

Spin light-emitting diodes (spin LEDs) [1,2] and spin lasers [3] have attracted significant interest in the last two decades because these devices can convert carrier spin polarization to circular polarization of light. Numerous applications are now being explored based on this technology, such as optical telecommunication with circular polarization [4,5], three-dimensional (3D) display screens [6], compact circular light sources for biologic applications [7] and quantum cryptography with circular polarized light emitted from a single quantum dot [8] etc. The spin LED devices consist of two parts: the ferromagnetic layer (spin injector), which is used to inject spin-polarized electrons (or holes) and the semiconductor part in which charge-carrier recombination takes place leading to the emission of circularly polarized light. To detect the optical circular polarization with a Faraday geometry (surface detection), the common way is to use a quantum-well- (QW) based LED structure according to the optical selection rule [9,10]. This allows, in principle, to obtain 100% of luminescence circular polarization if we inject 100% spin-polarized electrons in the LED structure (if spin relaxation is neglected in the semiconductor part). Low-dimensional structures such as quantum dots (QDs) also appear interesting because the spin-relaxation time was reported to be much larger than the one in QWs [11,12]. In particular, the doping of QDs plays an important role as it allows the control of the electron-hole exchange interaction [13]. When an electron is injected into a positively charged QD, the formation of a trion ($X^+$) minimizes the exchange

*yuan.lu@univ-lorraine.fr
†mathieu.stoffel@univ-lorraine.fr

 

interaction between electron and hole, which can result in long spin-relaxation time of electrons at low temperature (limited by the interaction of electrons with fluctuating nuclear spins) [12]. Several works have reported the electric spin injection in either InAs or (In, Ga)As QD-based spin LEDs [14–18] or spin lasers [19]. A significant electroluminescence (EL) circular polarization (approximately 5%) was measured even at room temperature with a magnetic field of 3 T [14].

The Co-Fe-B/MgO spin injector has shown very high spin-injection efficiencies [20,21]. By using an ultrathin Co-Fe-B/MgO structure, we have been able to obtain a perpendicularly magnetized spin injector, leading to the observation of a circular polarization at zero applied magnetic field [22–24], which is important for practical application. By using such a spin injector, a circular polarization as high as 35% for spin injection in a single QD was demonstrated [25]. The high electron spin injection also results in an efficient nuclear spin polarization. This has been identified from the nuclear spin-field-induced splitting in EL between the two circularly polarized states at zero magnetic field [25].

In this work, by taking benefits from such large circular polarization at zero magnetic field, we investigate the detailed spin-injection and spin-relaxation mechanisms in such a state-of-the-art sample. There are two key advantages for this kind of structure. Firstly, measurements without magnetic field prevents any magnetic field effect related to the Zeeman splitting [26] and the spin-relaxation mechanisms in the semiconductor part [18]. Secondly, a long spin-relaxation time in QDs can allow us to decouple the spin-relaxation process inside and outside of QDs. Here, the bias and temperature dependence of the circular polarization are systematically studied. We clearly evidence a two-step spin-relaxation process. The first step is related to the spin relaxation before electrons are trapped into QDs and the second step occurs inside the QDs before the recombination with holes. The understanding of spin-relaxation mechanisms helps to optimize the spin LED structure to achieve a better performance at room temperature and zero magnetic field.

## II. EXPERIMENTAL DETAILS

The spin LED structure contains two parts: one part is the semiconductor LED part and the other is the metallic spin-injector part. Figure 1 schematically shows the structure of the QD-based spin LED. The *p-i-n* LED device grown by MBE contains a single layer of $In_{0.3}Ga_{0.7}As$ quantum dots embedded in the active region. The full sequence of the structure is as follows: $p^+$-GaAs : Zn (001) substrate ($p = 3 \times 10^{18}$ cm$^{-3}$)/300 nm $p$-GaAs : Be ($p = 5 \times 10^{18}$ cm$^{-3}$)/400 nm $p$-$Al_{0.3}Ga_{0.7}As$ : Be ($p = 5 \times 10^{17}$–$5 \times 10^{18}$ cm$^{-3}$)/30 nm $i$-GaAs with Be $\delta$ doping in the center/7ML (In, Ga)As QD/30 nm $i$-GaAs/50 nm $n$-GaAs : Si ($n = 1 \times 10^{16}$ cm$^{-3}$). The bottom inset of Fig. 1 shows an AFM image of the (In, Ga)As/GaAs QD layer before capping with GaAs layer. The (In, Ga)As QDs have a density of $1.6 \times 10^{10}$ cm$^{-2}$. The average lateral dot diameter is about 30 nm and the height is about 9 nm. The Be $\delta$-doping concentration is calibrated to yield approximatively one hole per dot. The LED is passivated with arsenic in the MBE chamber. Subsequently, the structure is transferred through air into a second MBE-sputtering interconnected system. The As capping layer is desorbed at 300 °C in the MBE chamber and then the sample is transferred through ultrahigh vacuum to a sputtering chamber to grow the spin injector. The structure of the spin injector is as follows: 2.5 nm MgO/1.1 nm $Co_{0.4}Fe_{0.4}B_{0.2}$/5 nm Ta. To fabricate the devices, 300-$\mu$m diameter circular mesas are processed using standard UV photolithography and etching techniques. Finally, the processed wafers are cut into small pieces to perform rapid temperature annealing (RTA) at 300 °C for 3 min to establish the perpendicular magnetic anisotropy (PMA) of the spin injector. More details concerning the growth and the optimization of the perpendicular spin injector can be found in Refs [22,24].

## III. RESULTS AND DISCUSSIONS

### A. Structural characterization of the spin injector

High resolution scanning transmission electron microscopy (HRSTEM) is performed to characterize the interfacial structure of the spin injector after RTA treatment at 300 °C. The images are taken using a JEOL ARM200 cold field-emission gun operating at 200 KV. As shown in the top inset of Fig. 1, both MgO/GaAs and MgO/Co-Fe-B interfaces appear sharp. A thin amorphous GaAs layer (approximately 0.4 nm) is detected at the MgO/GaAs interface, which could be due to the large kinetic energy of the atoms reaching the surface during the sputtering growth process. The Ta layer remains almost amorphous after annealing. The MgO layer displays a good (001) textured structure and 11 atomic planes can be well distinguished. The high-quality MgO layer serves as a template to crystalize the above Co-Fe-B layer during annealing. The ultrathin Co-Fe-B layer (1.1 nm) is found to be homogenous and partially crystallized to bcc structure with an epitaxial relationship MgO[100](100)||Co-Fe[110](010). This result is in a good agreement with previous reports concerning the Co-Fe-B crystallization on magnetic tunnel junctions (MTJs) [27, 28]. Since the perpendicular magnetic anisotropy properties come from the interface anisotropy created by the hybridization of Fe(Co) and O atoms [22], the precise control of the MgO/Co-Fe-B interface structure and chemistry is essential to obtain PMA and high spin-injection efficiency [24].

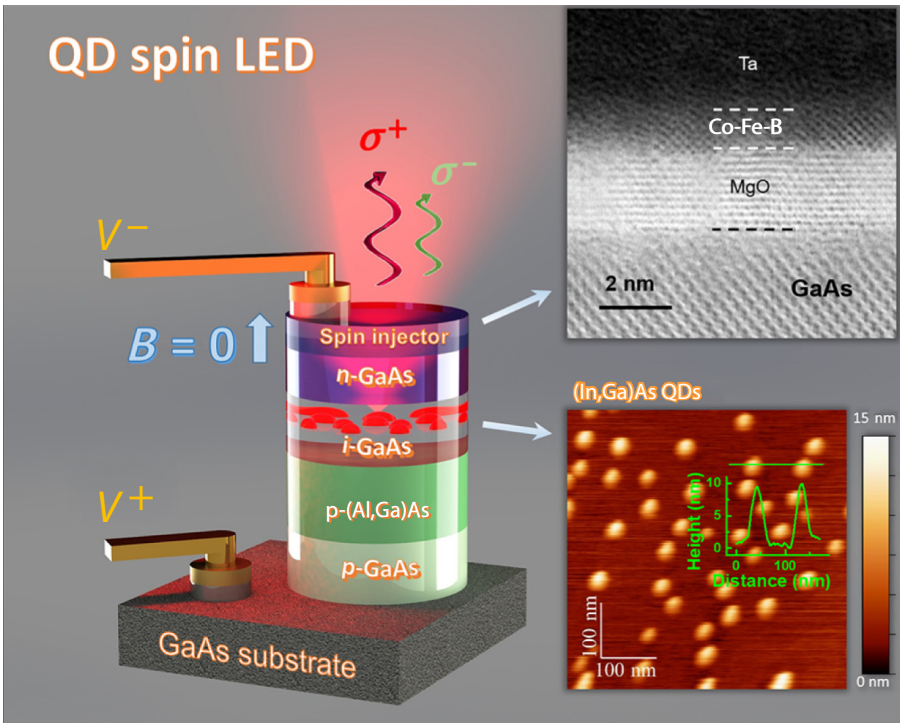


FIG. 1. Schematics of the stack structure of the QD-based spin LED, which can emit circularly polarized light at zero applied magnetic field. Upper inset: Brigth-field HRSTEM image of the spin-injector layer, which contains 5 nm Ta/1.1 nm Co-Fe-B/2.5 nm MgO. Lower inset: AFM image of the (In, Ga)As QD layer before capping with GaAs layer. The (In, Ga)As QDs have a density of $1.6 \times 10^{10}$ cm$^{-2}$. The inset of the AFM image shows the average lateral dot diameter of about 30 nm and the height of about 9 nm.

### B. Magnetic field dependence of circular polarization

For the electroluminescence measurements, the spin LED is mounted in a cryostat (developed by Cryoscan), which can be cooled down to 10 K with liquid helium. The EL signal is detected in a Faraday geometry with the magnetic field applied perpendicular to the sample plane. The EL signal is analyzed by a spectrometer (*i*HR 320) equipped with a 300 grooves/mm grating and detected by a Si-based CCD camera. The EL circular polarization $P_c$, which is defined as $P_c = (I^{\sigma+} - I^{\sigma-})/(I^{\sigma+} + I^{\sigma-})$, where $I^{\sigma+}$ and $I^{\sigma-}$ are the intensities of the right and left circularly polarized components of the luminescence, respectively, is analyzed through a $\lambda/4$ wave plate and a linear polarizer.

The insets of Fig. 2 show the typical polarization-resolved EL spectra measured from a spin LED at 10 K under a bias ($V_{\text{bias}}$) of 2.5 V with a very small current of 6 $\mu$A (current density of $1.4 \times 10^{-3}$ A/cm$^2$) at $B = 0$ T. In these spectra, we can observe a single peak centered at about 1.368 eV (wavelength of 906 nm) corresponding to the $X^+$ trion (one electron and two holes forming a singlet) transition for the quantum-dot ensemble. Due to the limitation of our spectrometer, the resolution in our spectra is not high enough to distinguish the EL signal originating from single quantum dot as published in Ref. [25]. The left and right insets correspond to the measurements where the sample magnetization is firstly saturated by positive and negative 0.35 T field, respectively. In both cases, we measure a large difference of the EL intensities for the right ($I^{\sigma+}$) and left ($I^{\sigma-}$) circularly polarized components at zero field. The EL $P_c$ can be determined to be about +18% and −19% in the left and right insets, respectively. The sign change of $P_c$ is due to the reversal

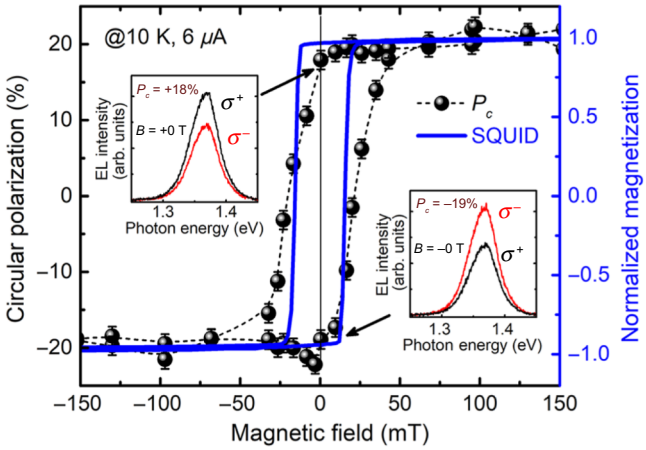


FIG. 2. Electroluminescence circular polarization $P_c$ (dashed lines with symbols) as a function of the out-of-plane magnetic field and corresponding SQUID hysteresis loop (blue solid line) measured at 10 K, respectively. The insets show the electroluminescence spectra measured at zero field, where $B = \pm 0$ T indicate that the sample magnetization is firstly saturated by a $\pm 0.35$ T field, respectively.

of the magnetization direction of the spin injector. Note that for such a thin Co-Fe-B layer, the spurious component due to the magnetic circular dichroism (MCD) that could artificially increase the measured $P_c$ is estimated to be less than 1%, based on measurements performed in Ref. [22]. We further examine the evolution of the EL circular polarization as a function of the magnetic field. As shown in Fig. 2, the behavior of $P_c$ as a function of magnetic field shows clear hysteresis loop feature, which can fairly match the magnetization hysteresis loop measured on the unpatterned sample by superconducting quantum interference device (SQUID). This gives a strong argument that the large remanent $P_c$ observed at $B = 0$ T is due to the injection of spin-polarized charge carriers from the ultrathin Co-Fe-B layer with PMA. The high $P_c$ measured at zero magnetic field in the QD spin LED is almost twice larger than our previous reported $P_c$ values in QW-based spin LED with the same type of PMA spin injector [24], and also approaches the high $P_c$ values reported with *in-plane* magnetized spin injectors [29–31]. This high-quality sample can be considered as a model system to study spin-injection and spin-relaxation mechanisms under zero magnetic field.

### C. Bias dependence of the circular polarization

In the following, we firstly investigate the bias-dependent EL circular polarization at 10 K. The inset of Fig. 3(a) presents a typical *I-V* characteristic of the spin LED device measured at 10 K. The current starts to increase when the bias exceeds 2 V. Figure 3(a) shows the evolution of the EL intensity as a function of the injected current. For low injected currents (<25 $\mu$A), the EL intensity first increases linearly. However, for currents larger than 25 $\mu$A, the EL intensity deviates from a linear behavior. The external quantum efficiency (EQE), which is defined by the ratio of the number of photons emitted from the QDs to the number of electrons passing through the device, decreases with the increasing bias. This can be explained by the filling of QD ground states under high current injection (saturation) [32]. As a consequence, more and more electrons contribute to radiative or nonradiative recombinations outside of the QD active region at larger bias. Figure 3(b) presents the EL spectra as a function of applied bias. A notable feature is that the shape of the spectra remains almost unchanged for different applied biases. The position of the EL peak maxima as indicated by the dashed line are always the same. Moreover, the FWHM of the spectra also remains constant at about 54 meV. All of these features indicate that the applied bias does not induce a quantum-confined Stark effect (QCSE) for the light emission from the QD [33]. Polarization-resolved spectra are acquired at different bias and the circular polarizations are extracted and presented in Fig. 3(c) as a function of applied bias and current. It is found that $P_c$ increases firstly with bias from 11% at 2 V to a maximum of 19% at 2.5 V and then decreases again to 11% at 4 V. The variation with current shows a much sharper increase of $P_c$ to the maximum, which is reached for a small current of 6 $\mu$A.

In order to understand the bias dependence, we perform a simulation of the band structure of the spin LED device by using a self-consistent "1D Poisson" program [34,35]. The nominal layer thicknesses and the dopant concentrations are input parameters for the simulation. For simplification, the $In_{0.3}Ga_{0.7}As$ QD layer is modeled by a 9-nm-thick $In_{0.3}Ga_{0.7}As$ QW layer. As shown in Fig. 3(d), for applied biases below 1 V, we find that the applied voltage mainly flattens the band in the GaAs depletion layer, leading to a flat-band condition in the LED. When the bias increases, the voltage starts to be applied on the MgO barrier without modifying the band structure of the semiconductor part. For all of the bias range considered here, the band structure of the $In_{0.3}Ga_{0.7}As$ active layer is almost unchanged, which is consistent with the fact that the EL peak position remains unchanged for different applied biases [Fig. 3(b)]. The left inset of Fig. 3(d) shows a linear increase of the calculated voltage across the MgO barrier when the applied bias is larger than 1 V. The voltage across the MgO results in a band bending in the MgO barrier, which has two consequences. Firstly, the Fermi level of the metallic injector is effectively lifted to be higher than the conduction-band minimum of GaAs, thus leading to the appearance of electroluminescence with a very small current injection [20,36]. Secondly, for larger applied biases, the injected electrons have a large kinetic energy after tunneling through the MgO barrier, as schematically shown in the right inset of Fig. 3(d). Concerning the EL circular polarization, the initial increase of $P_c$ is mainly due to the reduction of the electron transit time in the GaAs depletion layer. As reported for the electron spin injection in Si, the electron transit time can vary by 2 orders of magnitude from diffusion to drift regime [37]. The reduction of the transit time can effectively reduce the possibility of spin flipping due to the spin-relaxation mechanisms, mainly the Dyakonov-Perel (DP) mechanism [38], before electrons reach the active region. Therefore, the circular polarization increases for small applied biases. However, when the bias is too large, the electrons having high kinetic energy quickly lose their spin when they are thermalized to the conduction band. The rate of spin flipping $\tau_s^{-1}$ is proportional to $E_K^3$ [39]. Therefore, the circular polarization decreases for large applied biases. The nonmonotonic variation of $P_c$ reflects mainly the spin-relaxation mechanism before the electrons reach the active region. It is worthwhile to mention that for thin Schottky-barrier-based spin LED with a highly *n*-doped semiconductor layer at the interface, it is demonstrated that a very significant part of the bias drops in the semiconductor active zone. In that case, the dependence of circular polarization on bias

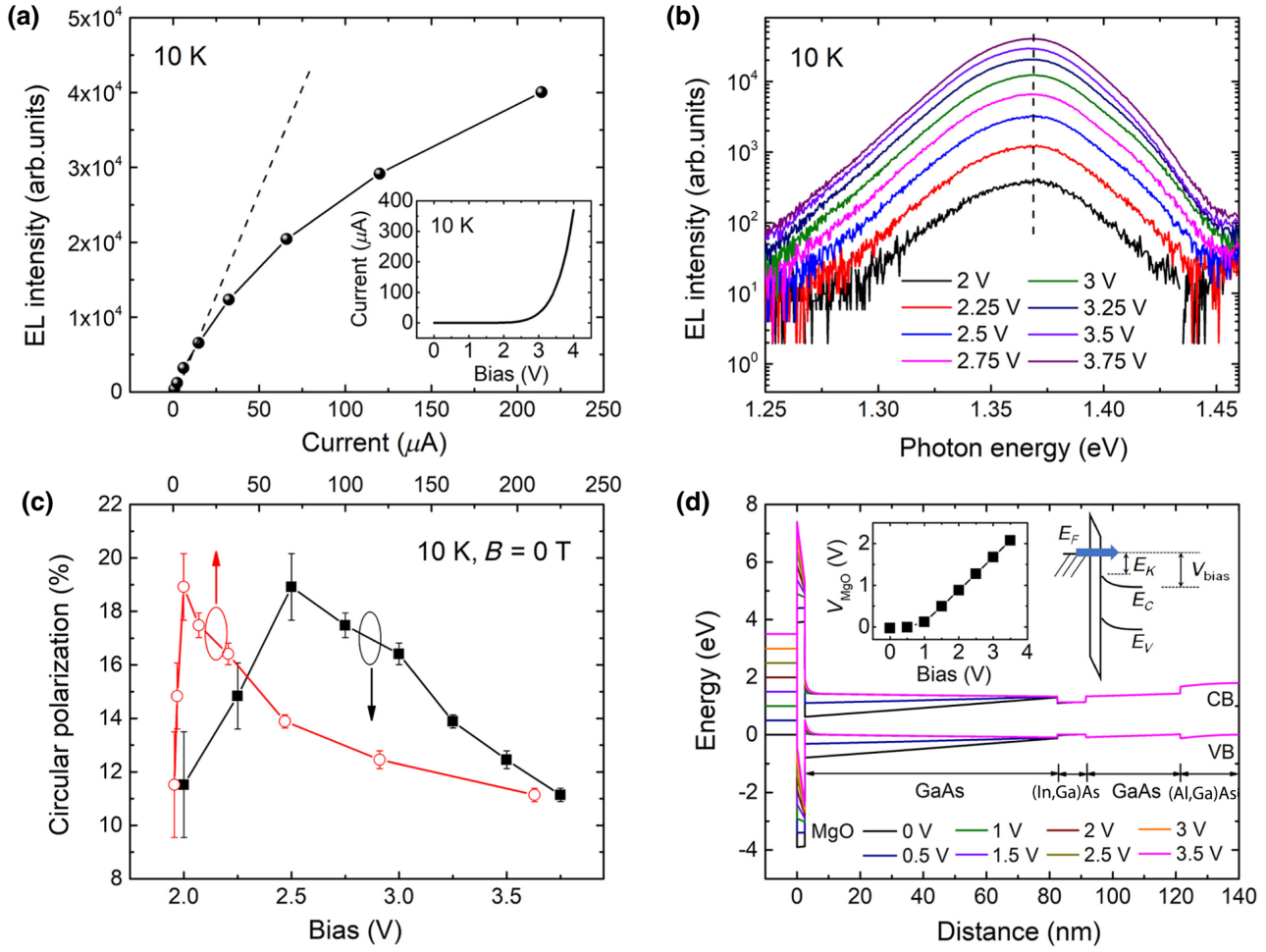


FIG. 3. (a) EL intensity as a function of the injection current at 10 K. Inset: $I$-$V_{\text{bias}}$ curve of the sample at 10 K. (b) EL spectra measured under different applied bias at 10 K. The photon energy corresponding to the peak maximum (marked by dashed line) shows negligible change as a function of biases. (c) EL circular polarization as a function of the injection current and applied bias at 10 K under zero field. (d) Band-structure calculations using a one-dimensional Poisson-Schrödinger solver at 10 K. Left inset: voltage drop on the MgO barrier ($V_{\text{MgO}}$) as a function of bias. Right inset: scheme of electron spin injection from the Fermi level of the metal to the conduction band of GaAs by tunneling through the MgO barrier. Due to the bias applied on the insulating barrier, the electrons have a certain kinetic energy ($E_k$) when arriving in the GaAs layer.

is usually explained by the complex bias dependence of the ratio $\tau/\tau_s$ between the carrier lifetime $\tau$ and the electron spin relaxation time $\tau_s$ in the active zone [31,40]. According to our simulations and experiments, this explanation does not hold for Co-Fe-B/MgO spin injector as the "flat-band" conditions remain even for large bias.

### D. Temperature dependence of the circular polarization

Let us now focus on the temperature dependence of the circular polarization. Figure 4(a) shows the EL intensity as a function of temperature measured for two fixed injected currents of 6 and 30 $\mu$A. The EL intensity decreases drastically with increasing temperature for both injection currents. Above 110 K, the EL intensity becomes too low to be detected. This drop of EL intensity is due to the thermal escape of carriers out of the QDs [41,42]. Here, this well-known effect is very pronounced since the (In, Ga)As QD emission peak (approximately 1.368 eV) in Fig. 3(b) is very close to the wetting-layer emission peak (approximately 1.409 eV), i.e., the dots are characterized by rather weak confinement energies compared to the self-organized quantum dots usually investigated [43].

The polarization-resolved spectra are then acquired to study the temperature dependence of $P_c$, as presented in Fig. 4(c) for both 6 and 30 $\mu$A injection currents. In comparison to the monotonic decrease of the EL intensity, the evolution of $P_c$ exhibits nonlinear variation with temperature: firstly $P_c$ decreases to reach a minimum at about 80 K and then $P_c$ increases from 80 up to 110 K. Below 60 K, $P_c$ measured for a 6 $\mu$A injection current is larger

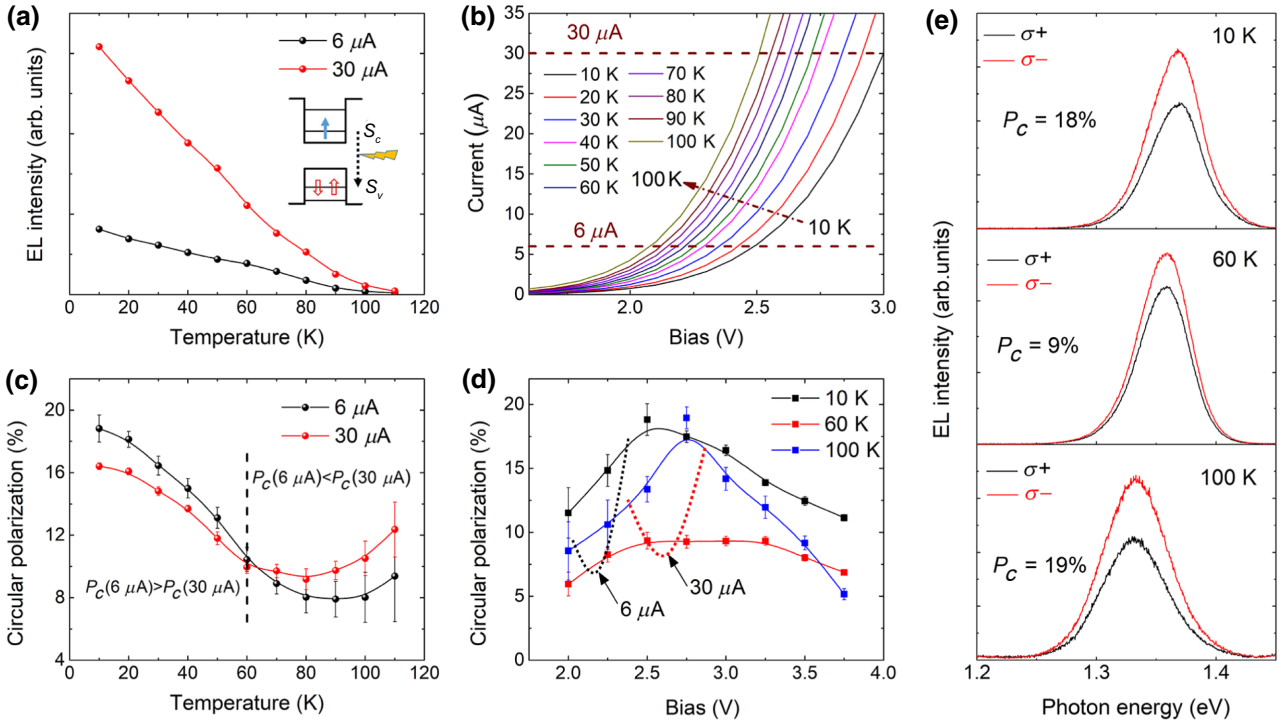


FIG. 4. (a) EL intensity as a function of temperature measured for fixed 6 $\mu$A (black dots) and 30 $\mu$A injection currents (red dots). Inset: scheme of a positively charged trion $X^+$ formed by one spin-polarized electron and two holes with opposite angular momentum projection. (b) *I-V* curves measured as a function of temperature ranging from 10 to 100 K. (c) $P_c$ as a function of temperature with fixed injection currents of 6 and 30 $\mu$A at zero magnetic field. (d) $P_c$ as a function of bias at 10, 60, and 100 K at zero magnetic field. (e) Polarization-resolved EL spectra at 10, 60, and 100 K at zero magnetic field with a fixed bias of 2.75 V.

than $P_c$ measured for a 30 $\mu$A injection current. For temperatures beyond 60 K, the opposite behavior is observed. To understand this temperature dependence, we measured the *I-V* characteristics of the spin LED device as a function of temperature [Fig. 4(b)]. The junction resistance, which consists of the MgO barrier and the semiconductor part, shows a decreasing behavior when the temperature increases from 10 to 100 K. For a constant injection current, the bias applied on the device decreases when the temperature increases. Therefore, the temperature dependence of $P_c$ at *a fixed current* is coupled with the bias dependence of $P_c$. To better understand the temperature dependence, we further measured the bias dependence of $P_c$ at three different temperatures (10, 60, and 100 K), as shown in Fig. 4(d). The bias dependences at 10 and 100 K show similar behavior. The small shift of the optimum bias to 2.75 V at 100 K is due to a small change of the resistance ratio between the MgO barrier and the semiconductor part at higher temperature. In contrast, $P_c$ depends less on the applied bias at 60 K. This agrees with the observation that $P_c$ values are almost the same for 6 and 30 $\mu$A injection current at 60 K [Fig. 4(c)]. As discussed above, the bias-dependent $P_c$ is mainly related to the band-structure change in the MgO barrier and GaAs depletion region. Therefore, studying the temperature dependence of $P_c$ at *a fixed voltage* can reveal the intrinsic spin-relaxation mechanism in the QD. Figure 4(e) shows the polarization-resolved EL spectra measured at 10, 60, and 100 K at $V_{\text{bias}} = 2.75$ V. With increasing temperature, the EL peak position shifts to lower photon energy and meanwhile the FWHM of the EL spectra increases. The measured $P_c$ firstly decreases from 18% at 10 K to 9% at 60 K, then increases again to 19% at 100 K. The increase of $P_c$ at higher temperature is much more pronounced than the measurement done at a fixed injection current. In Fig. 4(d), the dashed black and red lines intuitively show the evolution of $P_c$ with temperature for fixed injection currents of 6 and 30 $\mu$A, respectively, which allows us to easily understand the temperature-dependent behavior shown in Fig. 4(c).

Since the voltage partition between MgO and the semiconductor part is almost the same at 2.75 V by varying temperature, the temperature dependence of the circular polarization should unveil the spin dynamics, which occur after electrons are captured into the QD and before charge-carrier recombination. The EL circular polarization ($P_c$) can be related to the electron spin-polarization injected into QDs ($P_{\text{inj}}$) as

$$P_c = \alpha \times F \times P_{\text{inj}}, \tag{1}$$

where $F$ is expressed as $F = [1/(1 + \tau/\tau_s)]$ [44], $\tau$ and $\tau_s$ are the carrier lifetime and spin-relaxation time inside QDs, respectively. The parameter $\alpha$ (varying from 1 to 0) is linked to the average doping per quantum dot, which varies significantly when the temperature increases. This variation of QD doping is clearly identified in the temperature-dependent measurements of intersublevel absorption [45]. It has strong consequences on the amplitude of the measured EL circular polarization since the QD eigenstates change with the doping. It is well known that the exciton eigenstates of undoped (In, Ga)As quantum dots are linearly polarized due to the anisotropic exchange interaction [46]. As a consequence, electrically injecting a spin-polarized electron inside such a neutral quantum dot does not lead to the emission of circularly polarized luminescence in a cw measurement, i.e., $\alpha \sim 0$ [11,47]. However, if the QD contains a resident hole, the EL emitted by the spin LED reflects the spin polarization of the injected electron spin, i.e., $\alpha \sim 1$. Indeed, the eigenstates of the charged exciton [one electron and two holes forming a singlet, as shown in the inset of Fig. 4(a)] are circularly polarized: the exchange interaction between electron and holes vanish [46]. This means that the average $p$-doping per QD in the spin LED device plays a crucial role on the amplitude of the measured circularly polarized EL independently of the electron and spin lifetimes.

The decrease of the EL circular polarization from 10 to 80 K observed in Fig. 4(c) can be explained by Eq. (1). In this temperature range, the investigations in spin LED based on quantum wells show that $P_{\text{inj}}$ varies very weakly [22]. Moreover, it is shown that the electron spin-relaxation time $\tau_s$ from a single InAs QD trion is also almost constant from 0 to 50 K [48]. As a consequence, the $P_c$ decrease in Fig. 4(c) can be related either to an increase of the lifetime $\tau$ or to a decrease of $\alpha$ due to the doping variation of the dot. The lifetime increase in the QD is very unlikely when the temperature increases. Thus we interpret the drop of $P_c$ as a consequence of the reduction of $\alpha$ (optimized to be close to 1 at 10 K). This interpretation is fully consistent with the EL quenching presented in Fig. 4(a), which results from the thermal escape of the holes from the QDs. For temperatures above 80 K, we observe an increase of $P_c$ in Fig. 4(c). This could be due to a decrease of the electron lifetime resulting from the electron escape from the quantum dots. Since the energy difference for electrons between the QD ground state and the wetting-layer states is larger compared to the one for holes [see inset of Fig. 4(a)], it explains that this effect occurs at higher temperatures [45,49].

By investigating the spin injection in a nominally *undoped* (In, Ga)As QD spin LED, Li *et al.* [14] reported that $P_c$ (approximately 5% for $B = 3$ T) is almost constant and can be measured even at room temperature. The difference with our work could rely on the characteristics of the (In, Ga)As quantum dots characterized in this reference by much weaker thermal escape of carriers thanks to a better confinement of carriers (emission wavelengths of the quantum dots beyond 1 $\mu$m).

### E. Two-step spin-relaxation process

A notable result from this work is the clear evidence of a two-step spin-relaxation process. The first step occurs when electrons tunnel through the MgO barrier and travel across the GaAs depletion layer, which is manifested by a bias-dependent $P_c$ measurement. The second step occurs when electrons are captured into QDs prior to their recombination with holes, which is manifested by a temperature-dependent $P_c$ measurement. The two steps can be decoupled and expressed by the following relationship:

$$P_c = \alpha \times F \times P_{\text{inj}} = \gamma(T) \times \eta(V) \times P_e, \qquad (2)$$

where $\eta$ characterizes the spin relaxation in the first step (which depends on the bias) and $\gamma$ characterizes the spin dynamics in the QD (which depends on the temperature). $P_e$ represents the spin-injection efficiency when an electron enters into the semiconductor part. Let us focus on four different $P_c$ values measured at 10 and 60 K and under applied biases of 2 and 2.5 V. At 10 K and 2 V, the spin relaxation is mainly controlled by the first process yielding $P_c$ (10 K, 2 V) = 11.5%. At 10 K and 2.5 V, the spin relaxation is minimized yielding the highest $P_c$ (10 K, 2.5 V) = 18.8%. At 60 K and 2 V, the two mechanisms are coming into play, thus resulting in the minimum $P_c$ (60 K, 2 V) = 5.9%. At 60 K and 2.5 V, the spin relaxation in the QD dominates, thus giving a $P_c$ (60 K, 2.5 V) = 9.3%. It is worth mentioning that the product of $P_c$ (10 K, 2.5 V) and $P_c$ (60 K, 2 V) is almost equal to the product of $P_c$ (10 K, 2 V) and $P_c$ (60 K, 2.5 V), which provides a strong argument of the two-step spin-relaxation process following Eq. (2).

Thanks to the highly efficient spin injection and long spin-relaxation time in $p$-doped QDs at zero magnetic field, we are able to provide evidence of a two-step spin-relaxation process. In previous studies, the large magnetic field (several teslas) used for spin LED with the *in-plane* magnetized spin injector can lead to multiple spurious effects, which modify the electron spin dynamics. Firstly, the Zeeman effect can split energy levels in the semiconductor and thus induce EL circular polarization [26]. Secondly, the magnetic field can polarize the nuclear spin and reduce the spin relaxation related to the electron-nuclear hyperfine interaction [12]. Thirdly, the large magnetic field can also affect the DP mechanism, thus increasing the spin-diffusion length and the spin lifetime in the semiconductor part [18]. The long spin-relaxation time in our system is linked to the intrinsically long spin relaxation of time of the electron within the positively charged exciton and the dynamical polarization of nuclear spins [11,12]. In our previous work [25], we have measured a nuclear field of about 200 mT generated by the nuclear spin polarization at

zero magnetic field after electron spin injection. This large nuclear field can protect the electron spin polarization and effectively enhance the spin-relaxation time.

### F. Comparison of QD spin LED with QW spin LED

Finally, we make a comparison between QD- and QW-based spin LEDs having the same Co-Fe-B/MgO PMA spin injector. The investigated QW-based spin LED is characterized by a 10-nm-thick undoped $In_{0.1}Ga_{0.9}As$ QW in the active region. The distance between the injector and the active region is about 100 nm instead of 80 nm for the QD-based spin LED, but this effect should be negligible since the spin-diffusion length is much longer than 20 nm at 10 K (approximately 3 $\mu$m [50]). This allows us to compare the spin-relaxation mechanism only in the different active regions. In the QW system, we measured a $P_c$ of 8%–10% (depending on samples) at 10 K under optimized bias condition [24]. By considering the value of $P_c$ measured in this work at the optimum bias (i.e., 19%), we find that it is almost twice larger as that obtained for the QW-based spin LED. This comparison validates the superior performance of QD-based spin LED compared to QW-based spin LED even by using exactly the same spin injector. This superiority is mainly due to, as said previously, longer spin-relaxation times for electrons in $p$-doped quantum dots compared to quantum wells, in particular when dynamic nuclear polarization occurs in cw regime, which induces a nuclear field that protects the electron spin polarization. Finally, we also emphasize that the large circular polarization (19%) combined with very low power consumption of 15 $\mu$W (with a current density of about $1.4 \times 10^{-3}$ A/cm$^2$) offers a great advantage of QD-based spin LED for future spin-optoelectronic applications. Large EL circular polarization at room temperature should be obtained using quantum dots with stronger confinement energies in order to reduce the thermal escape of carriers. It is also worth mentioning that although Be is an excellent acceptor, its diffusivity hinders a real $\delta$ doping [51]. Carbon is a better candidate for $\delta$ doping to yield a better temperature performance, which is not amphoteric and has no noticeable diffusion [52].

## IV. CONCLUSIONS

In conclusion, we study the spin-injection and spin-relaxation mechanism in $p$-doped (In, Ga)As QD-based spin LED under zero applied magnetic field. We measure a large circular polarization of 19% up to 100 K in remanence with optimized bias condition. We systematically study the bias and temperature dependence of the circular polarization and evidenced a two-step spin-relaxation process. The first step occurs when electrons tunnel through the MgO barrier and travel across the GaAs depletion layer. The spin relaxation is determined by the kinetic energy of the injected electrons and the transit time though the GaAs layer, as manifested by the bias-dependent $P_c$. The second step occurs in the QDs prior to electron recombination with holes. The circular polarization is determined by the average doping in the QDs together with the ratio of electron lifetime and spin-relaxation time, as manifested by the temperature-dependent $P_c$. In addition, we prove the superior performance of QD-based spin LEDs compared to QW-based spin LEDs having the same spin injector thanks to the longer electron spin-relaxation times in $p$-doped quantum dots. This study paves the way for the development of high-performance QD-based spin LEDs at room temperature without applied magnetic field, which is essential for many spin-optoelectronic applications such as optical memory element [53] and optical telecommunication with circular polarization [5].

## ACKNOWLEDGMENTS

We thank Michel Hehn for his help with the development of ultrathin PMA Co-Fe-B by sputtering. This work is supported by the joint French National Research Agency (ANR)-National Natural Science Foundation of China (NSFC) SISTER Project (Grants No. ANR-11-IS10-0001 and No. NNSFC 61161130527), ANR FEOrgSpin project (Grant No. ANR-18-CE24-0017) and ANR SIZMO2D project (Grant No. ANR-19-CE24-0005). We also acknowledge the PHC CAI YUANPEI 2017 (No. 38917YJ) program, ICEEL (INTER-Carnot) Blue-SpinLED and ICEEL (international) SHATIPN projects as well as the French PIA project "Lorraine Universite d'Excellence" (Grant No. ANR-15-IDEX-04-LUE). Experiments are performed using equipment from the platform TUBE-Davm funded by FEDER (EU), ANR, the Region Lorraine and Grand Nancy. X.M. acknowledges the Institut Universitaire de France.

[1] R. Fiederling, M. Keim, G. Reuscher, W. Ossau, G. Schmidt, A. Waag, and L. W. Molenkamp, Injection and detection of a spin-polarized current in a light-emitting diode, Nature **402**, 787 (1999).

[2] Y. Ohno, D. K. Young, B. Beschoten, F. Matsukura, H. Ohno, and D. D. Awschalom, Electrical spin injection in a ferromagnetic semiconductor heterostructure, Nature **402**, 790 (1999).

[3] M. Holub, J. Shin, S. Chakrabarti, and P. Bhattacharya, Electrically injected spin-polarized vertical-cavity surface-emitting lasers, Appl. Phys. Lett. **87**, 091108 (2005).

[4] R. Farshchi, M. Ramsteiner, J. Herfort, A. Tahraoui, and H. T. Grahn, Optical communication of spin information between light emitting diodes, Appl. Phys. Lett. **98**, 162508 (2011).

[5] M. Lindemann, G. Xu, T. Pusch, R. Michalzik, M. R. Hofmann, I. Žutić, and N. C. Gerhardt, Ultrafast spin-lasers, Nature **568**, 212 (2019).

[6] D.-Y. Kim, Potential application of spintronic light-emitting diode to binocular vision for three-dimensional display technology, J. Korean Phys. Soc. **49**, 4 (2006).

[7] B. Kunnen, C. Macdonald, A. Doronin, S. Jacques, M. Eccles, and I. Meglinski, Application of circularly polarized light for non-invasive diagnosis of cancerous tissues and turbid tissue-like scattering media, J. Biophotonics **8**, 317 (2015).

[8] P. Asshoff, A. Merz, H. Kalt, and M. Hetterich, A spintronic source of circularly polarized single photons, Appl. Phys. Lett. **98**, 112106 (2011).

[9] F. Meier and B. P. Zakharchenya, *Optical Orientation* (North-Holland, Amsterdam, The Netherlands, 1984).

[10] M. I. Dyakonov, *Spin Physics in Semiconductors* (Springer, Berlin Heidelberg, 2008).

[11] M. Paillard, X. Marie, P. Renucci, T. Amand, A. Jbeli, and J. M. Gérard, Spin Relaxation Quenching in Semiconductor Quantum Dots, Phys. Rev. Lett. **86**, 1634 (2001).

[12] P. F. Braun, X. Marie, L. Lombez, B. Urbaszek, T. Amand, P. Renucci, V. K. Kalevich, K. V. Kavokin, O. Krebs, P. Voisin, and Y. Masumoto, Direct Observation of the Electron Spin Relaxation Induced by Nuclei in Quantum Dots, Phys. Rev. Lett. **94**, 116601 (2005).

[13] A. S. Bracker, E. A. Stinaff, D. Gammon, M. E. Ware, J. G. Tischler, A. Shabaev, A. L. Efros, D. Park, D. Gershoni, V. L. Korenev, and I. A. Merkulov, Optical Pumping of the Electronic and Nuclear Spin of Single Charge-Tunable Quantum Dots, Phys. Rev. Lett. **94**, 047402 (2005).

[14] C. H. Li, G. Kioseoglou, O. M. J. van't Erve, M. E. Ware, D. Gammon, R. M. Stroud, B. T. Jonker, R. Mallory, M. Yasar, and A. Petrou, Electrical spin pumping of quantum dots at room temperature, Appl. Phys. Lett. **86**, 132503 (2005).

[15] G. Itskos, E. Harbord, S. K. Clowes, E. Clarke, L. F. Cohen, R. Murray, P. V. Dorpe, and W. V. Roy, Oblique Hanle measurements of InAs/GaAs quantum dot spin-light emitting diodes, Appl. Phys. Lett. **88**, 022113 (2006).

[16] L. Lombez, P. Renucci, P. F. Braun, H. Carrère, X. Marie, T. Amand, B. Urbaszek, J. L. Gauffier, P. Gallo, T. Camps, A. Arnoult, C. Fontaine, C. Deranlot, R. Mattana, H. Jaffrès, J.-M. George, and P. H. Binh, Electrical spin injection into p-doped quantum dots through a tunnel barrier, Appl. Phys. Lett. **90**, 081111 (2007).

[17] H. Soldat, M. Li, N. C. Gerhardt, M. R. Hofmann, A. Ludwig, A. Ebbing, D. Reuter, A. D. Wieck, F. Stromberg, W. Keune, and H. Wende, Room temperature spin relaxation length in spin light-emitting diodes, Appl. Phys. Lett. **99**, 051102 (2011).

[18] H. Höpfner, C. Fritsche, A. Ludwig, A. Ludwig, F. Stromberg, H. Wende, W. Keune, D. Reuter, A. D. Wieck, N. C. Gerhardt, and M. R. Hofmann, Magnetic field dependence of the spin relaxation length in spin light-emitting diodes, Appl. Phys. Lett. **101**, 112402 (2012).

[19] D. Basu, D. Saha, C. C. Wu, M. Holub, Z. Mi, and P. Bhattacharya, Electrically injected InAs/GaAs quantum dot spin laser operating at 200 K, Appl. Phys. Lett. **92**, 091119 (2008).

[20] Y. Lu, V. G. Truong, P. Renucci, M. Tran, H. Jaffrès, C. Deranlot, J.-M. George, A. Lemaître, Y. Zheng, D. Demaille, P.-H. Binh, T. Amand, and X. Marie, MgO thickness dependence of spin injection efficiency in spin-light emitting diodes, Appl. Phys. Lett. **93**, 152102 (2008).

[21] P. Barate, S. Liang, T. T. Zhang, J. Frougier, M. Vidal, P. Renucci, X. Devaux, B. Xu, H. Jaffrès, J. M. George, X. Marie, M. Hehn, S. Mangin, Y. Zheng, T. Amand, B. Tao, X. F. Han, Z. Wang, and Y. Lu, Electrical spin injection into InGaAs/GaAs quantum wells: A comparison between MgO tunnel barriers grown by sputtering and molecular beam epitaxy methods, Appl. Phys. Lett. **105**, 012404 (2014).

[22] S. H. Liang, et al., Large and robust electrical spin injection into GaAs at zero magnetic field using an ultrathin CoFeB/MgO injector, Phys. Rev. B **90**, 085310 (2014).

[23] B. S. Tao, P. Barate, J. Frougier, P. Renucci, B. Xu, A. Djeffal, H. Jaffrès, J.-M. George, X. Marie, S. Petit-Watelot, S. Mangin, X. F. Han, Z. G. Wang, and Y. Lu, Electrical spin injection into GaAs based light emitting diodes using perpendicular magnetic tunnel junction-type spin injector, Appl. Phys. Lett. **108**, 152404 (2016).

[24] B. Tao, P. Barate, X. Devaux, P. Renucci, J. Frougier, A. Djeffal, S. Liang, B. Xu, M. Hehn, H. Jaffrès, J.-M. George, X. Marie, S. Mangin, X. Han, Z. Wang, and Y. Lu, Atomic-scale understanding of high thermal stability of the Mo/CoFeB/MgO spin injector for spin-injection in remanence, Nanoscale **10**, 10213 (2018).

[25] F. Cadiz, et al., Electrical initialization of electron and nuclear spins in a single quantum dot at zero magnetic field, Nano Lett. **18**, 2381 (2018).

[26] P. Renucci, V. G. Truong, H. Jaffrès, L. Lombez, P. H. Binh, T. Amand, J. M. George, and X. Marie, Spin-polarized electroluminescence and spin-dependent photocurrent in hybrid semiconductor/ferromagnetic heterostructures: An asymmetric problem, Phys. Rev. B **82**, 195317 (2010).

[27] S. Ikeda, K. Miura, H. Yamamoto, K. Mizunuma, H. D. Gan, M. Endo, S. Kanai, J. Hayakawa, F. Matsukura, and H. Ohno, A perpendicular-anisotropy CoFeB—MgO magnetic tunnel junction, Nat. Mater. **9**, 721 (2010).

[28] Y. Lu, C. Deranlot, A. Vaurès, F. Petroff, J.-M. George, Y. Zheng, and D. Demailles, Effects of a thin Mg layer on the structural and magnetoresistance properties of CoFeB/MgO/CoFeB magnetic tunnel junctions, Appl. Phys. Lett. **91**, 222504 (2007).

[29] X. Jiang, R. Wang, R. M. Shelby, R. M. Macfarlane, S. R. Bank, J. S. Harris, and S. S. P. Parkin, Highly Spin-Polarized Room-Temperature Tunnel Injector for Semiconductor Spintronics Using MgO(100), Phys. Rev. Lett. **94**, 056601 (2005).

[30] C. H. Li, G. Kioseoglou, A. T. Hanbicki, R. Goswami, C. S. Hellberg, B. T. Jonker, M. Yasar, and A. Petrou, Electrical spin injection into the InAs/GaAs wetting layer, Appl. Phys. Lett. **91**, 262504 (2007).

[31] C. Adelmann, X. Lou, J. Strand, C. J. Palmstrøm, and P. A. Crowell, Spin injection and relaxation in ferromagnet-semiconductor heterostructures, Phys. Rev. B **71**, 121301(R) (2005).

[32] V. K. Kalevich, M. Paillard, K. V. Kavokin, X. Marie, A. R. Kovsh, T. Amand, A. E. Zhukov, Y. G. Musikhin, V. M. Ustinov, E. Vanelle, and B. P. Zakharchenya, Spin redistribution due to Pauli blocking in quantum dots, Phys. Rev. B **64**, 045309 (2001).

[33] D. A. B. Miller, D. S. Chemla, T. C. Damen, A. C. Gossard, W. Wiegmann, T. H. Wood, and C. A. Burrus, Band-edge Electroabsorption in Quantum Well Structures: The Quantum-Confined Stark Effect, Phys. Rev. Lett. **53**, 2173 (1984).

[34] G. L. Snider, I. H. Tan, and E. L. Hu, Electron states in mesa-etched one-dimensional quantum well wires, J. Appl. Phys. **68**, 2849 (1990).

[35] I. H. Tan, G. L. Snider, L. D. Chang, and E. L. Hu, A self-consistent solution of Schrödinger–Poisson equations using a nonuniform mesh, J. Appl. Phys. **68**, 4071 (1990).

[36] P. Barate, et al., Bias Dependence of the Electrical Spin Injection Into GaAs From Co-Fe-B/MgO Injectors with Different MgO Growth Processes, Phys. Rev. Appl. **8**, 054027 (2017).

[37] Y. Lu and I. Appelbaum, Reverse Schottky-asymmetry spin current detectors, Appl. Phys. Lett. **97**, 162501 (2010).

[38] M. I. Dyakonov and V. I. Perel, Spin orientation of electrons associated with the interband absorption of light in semiconductors, J. Exp. Theor. Phys **33**, 1053 (1971).

[39] P. H. Song and K. W. Kim, Spin relaxation of conduction electrons in bulk III-V semiconductors, Phys. Rev. B **66**, 035207 (2002).

[40] C. Adelmann, J. L. Hilton, B. D. Schultz, S. McKernan, C. J. Palmstrøm, X. Lou, H.-S. Chiang, and P. A. Crowell, Spin injection from perpendicular magnetized ferromagnetic $\delta$-MnGa into (Al, Ga)As heterostructures, Appl. Phys. Lett. **89**, 112511 (2006).

[41] D. I. Lubyshev, P. P. Gonzalez-Borrero, E. Marega Jr., E. Petitprez, N. La Scala Jr., and P. Basmaji, Exciton localization and temperature stability in self-organized InAs quantum dots, Appl. Phys. Lett. **68**, 205 (1996).

[42] D. P. Popescu, P. G. Eliseev, A. Stintz, and K. J. Malloy, Temperature dependence of the photoluminescence emission from InAs quantum dots in a strained $Ga_{0.85}In_{0.15}As$ quantum well, Semicond. Sci. Technol. **19**, 33 (2004).

[43] M. Grundmann, O. Stier, and D. Bimberg, Inas/GaAs pyramidal quantum dots: Strain distribution, optical phonons, and electronic structure, Phys. Rev. B **52**, 11969 (1995).

[44] B. L. Liu, P. Renucci, H. Carrère, M. Sénès, X. Marie, T. Amand, J. F. Bobo, C. Fontaine, A. Arnoult, and P. H. Binh, Spin injection probed by combined optical and electrical techniques in spin-LED, Phys. Status Solidi (c) **1**, 475 (2004).

[45] F. Bras, P. Boucaud, S. Sauvage, and G. Fishman, Temperature dependence of intersublevel absorption in InAs/GaAs self-assembled quantum dots, Appl. Phys. Lett. **80**, 4620 (2002).

[46] M. Bayer, G. Ortner, O. Stern, A. Kuther, A. A. Gorbunov, A. Forchel, P. Hawrylak, S. Fafard, K. Hinzer, T. L. Reinecke, S. N. Walck, J. P. Reithmaier, F. Klopf, and F. Schäfer, Fine structure of neutral and charged excitons in self-assembled In(Ga)As/(Al)GaAs quantum dots, Phys. Rev. B **65**, 195315 (2002).

[47] R. I. Dzhioev, B. P. Zakharchenya, E. L. Ivchenko, V. L. Korenev, Y. G. Kusraev, N. N. Ledentsov, V. M. Ustinov, A. E. Zhukov, and A. F. Tsatsulnikov, Optical orientation and alignment of excitons in quantum dots, Phys. Solid State **40**, 790 (1998).

[48] X. M. Dou, B. Q. Sun, D. S. Jiang, H. Q. Ni, and Z. C. Niu, Temperature dependence of electron-spin relaxation in a single InAs quantum dot at zero applied magnetic field, J. Appl. Phys. **111**, 053524 (2012).

[49] A. J. Williamson, L. W. Wang, and A. Zunger, Theoretical interpretation of the experimental electronic structure of lens-shaped self-assembled InAs/GaAs quantum dots, Phys. Rev. B **62**, 12963 (2000).

[50] G. Salis, A. Fuhrer, R. R. Schlittler, L. Gross, and S. F. Alvarado, Temperature dependence of the nonlocal voltage in an Fe/GaAs electrical spin-injection device, Phys. Rev. B **81**, 205323 (2010).

[51] R. Mosca, P. Bussei, S. Franchi, P. Frigeri, E. Gombia, A. Carnera, and M. Peroni, Be diffusion in molecular beam epitaxy grown GaAs structures, J. Appl. Phys. **93**, 9709 (2003).

[52] L. Winking, M. Wenderoth, T. C. G. Reusch, R. G. Ulbrich, P.-J. Wilbrandt, R. Kirchheim, S. Malzer, and G. Döhler, Ideal delta doping of carbon in GaAs, J. Vac. Sci. Technol. B **23**, 267 (2005).

[53] T. Alexoudi, G. T. Kanellos, and N. Pleros, Optical RAM and integrated optical memories: A survey, Light Sci. Appl. **9**, 91 (2020).